

## Measurement of the secondary electron emission from CVD diamond films using phosphor screen detectors

This content has been downloaded from IOPscience. Please scroll down to see the full text.

2015 JINST 10 P03004

(<http://iopscience.iop.org/1748-0221/10/03/P03004>)

View [the table of contents for this issue](#), or go to the [journal homepage](#) for more

Download details:

IP Address: 137.222.43.33

This content was downloaded on 03/03/2015 at 16:57

Please note that [terms and conditions apply](#).

# Measurement of the secondary electron emission from CVD diamond films using phosphor screen detectors

R. Vaz,<sup>a</sup> P.W. May,<sup>a,1</sup> N.A. Fox,<sup>a</sup> C.J. Harwood,<sup>b</sup> V. Chatterjee,<sup>a</sup> J.A. Smith,<sup>a</sup>  
C.J. Horsfield,<sup>c</sup> J.S. Lapington<sup>d</sup> and S. Osbourne<sup>a</sup>

<sup>a</sup>*School of Chemistry, University of Bristol,  
Bristol BS8 1TS, U.K.*

<sup>b</sup>*Department of Physics, H. H. Wills Physics Laboratory,  
University of Bristol, U.K.*

<sup>c</sup>*AWE,  
Aldermaston, Reading, RG7 4PR*

<sup>d</sup>*Space Research Centre, University of Leicester,  
University Road, Leicester, LE1 7RH, U.K.*

*E-mail:* [paul.may@bristol.ac.uk](mailto:paul.may@bristol.ac.uk)

**ABSTRACT:** Diamond-based photomultipliers have the potential to provide a significant improvement over existing devices due to diamond's high secondary electron yield and narrow energy distribution of secondary electrons which improves energy resolution creating extremely fast response times. In this paper we describe an experimental apparatus designed to study secondary electron emission from diamond membranes only 400 nm thick, observed in reflection and transmission configurations. The setup consists of a system of calibrated P22 green phosphor screens acting as radiation converters which are used in combination with photomultiplier tubes to acquire secondary emission yield data from the diamond samples. The superior signal voltage sampling of the phosphor screen setup compared with traditional Faraday Cup detection allows the variation in the secondary electron yield across the sample to be visualised, allowing spatial distributions to be obtained. Preliminary reflection and transmission yield data are presented as a function of primary electron energy for selected CVD diamond films and membranes. Reflection data were also obtained from the same sample set using a Faraday Cup detector setup. In general, the curves for secondary electron yield versus primary energy for both measurement setups were comparable. On average a 15–20% lower signal was recorded on our setup compared to the Faraday Cup, which was attributed to the lower photoluminescent efficiency of the P22 phosphor screens when operated at sub-kilovolt bias voltages.

**KEYWORDS:** Secondary electron emitters and dynodes and their production; Diamond Detectors

<sup>1</sup>Corresponding author.



---

## Contents

<b>1</b>	<b>Introduction</b>	<b>1</b>
<b>2</b>	<b>Experimental</b>	<b>3</b>
2.1	Faraday cup system	3
2.2	New Phosphor Screen system	5
2.2.1	Measurement procedure — reflection mode	10
2.2.2	Measurement procedure – transmission mode	12
2.3	CVD Diamond test samples	12
<b>3</b>	<b>Results</b>	<b>13</b>
3.1	SEY measured in Reflection Mode	13
3.2	SEY measured in Transmission Mode	14
<b>4</b>	<b>Conclusions</b>	<b>15</b>

---

## 1 Introduction

Electron emission is a fundamental phenomenon associated with most interactions of energetic particles with solid surfaces, and its measurement in areas such as radiation biology [1], particle detectors [2], microscopy and surface analysis [3] is extremely important. Light emission is usually measured by focusing the emitted photons onto a photocathode which then emits electrons which can be collected and measured as an electrical current. At low photon fluxes, the small number of emitted electrons must be multiplied in order to obtain a usable signal. This multiplication is usually achieved by dynode devices, such as the ones used in photomultiplier tubes (PMTs) or microchannel plates (MCPs), which use high voltages to accelerate the electrons onto surfaces with a high ( $> 1$ ) secondary electron emission yield (SEY). For these surfaces, the primary-electron impacts liberate a number of secondary electrons depending on the dynode material, which are then accelerated deeper into the device to strike another dynode surface, which, in turn, emit yet more electrons. Most electron-multiplication devices require many such stages, the number of which is determined by the SEY of each surface and the required gain. Hence, using a dynode material with the highest possible SEY reduces the number of multiplication stages required, making the device simpler and cheaper.

Dynode devices usually operate in one of two modes, reflection or transmission (see figure 1). In reflection mode the secondary electrons are emitted from the same surface that is struck by the primary electron beam. Due to the nature of the collision cascade, the electrons are emitted in all directions in a hemisphere around the impact point, with energies typically  $< 20$  eV. Commercial multiple-stage reflective dynode devices often follow a ‘Venetian blind’ design, with a series of slanted dynode surfaces with increasing positive bias values, arranged such that emitted secondary

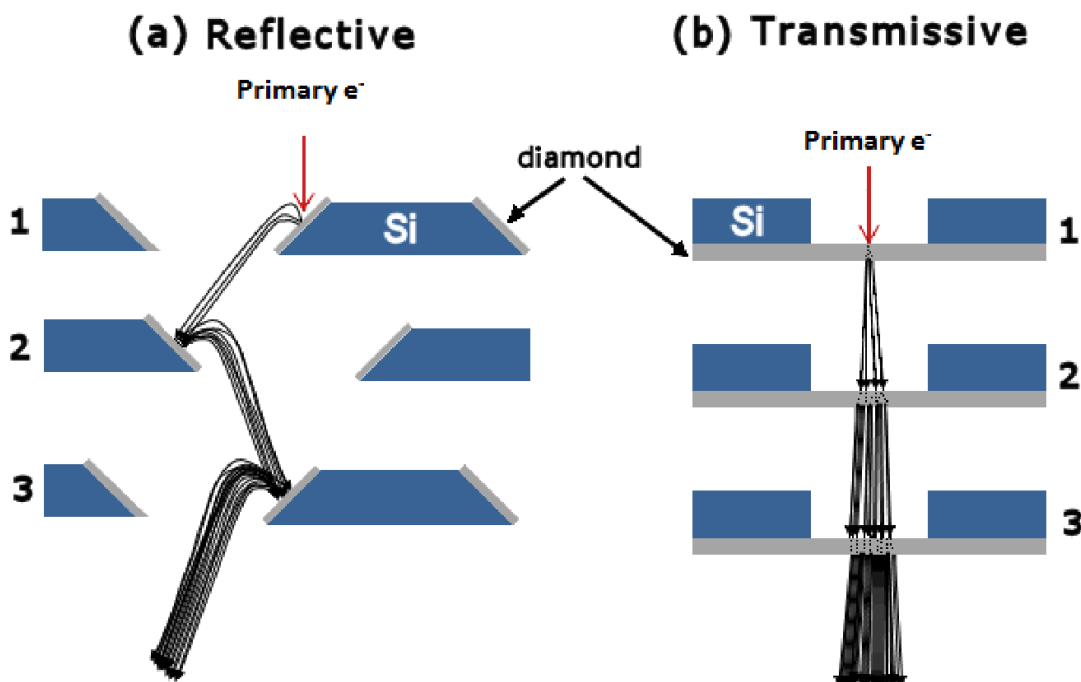


**Figure 1.** Two geometries typically used for secondary electron multiplication dynode devices, except here using thin film diamond as the dynode material. Three multiplication stages are shown for each, with each stage having a higher positive bias compared to the previous stage. (a) ‘Venetian blind’-style reflective device. (b) A transmissive device involving thin membranes.

electrons are attracted downwards onto the next surface. The slanted surfaces in each layer are offset such that there is no direct line-of-sight for the primary beam to the final detector.

In contrast, in a transmissive device the secondary electrons are emitted from the opposite surface to that which is struck by the primary electron beam. This requires that the material be thin enough (typically  $\ll 1 \mu\text{m}$ ) to allow the electron beam to pass through it, and has the advantage that no complicated geometries are required — stacking the dynode membranes on top of each other is sufficient. However, some secondary electrons are lost in reflection at each stage, and it may be necessary to have different surface treatments (such as surface functionalisation) on the top and bottom surfaces to reduce and increase SEY, respectively.

Secondary electron emission is generally interpreted as a three-step process, in which the excitation of the emitted electrons, their transport to the solid surface and their escape into the vacuum are described by three different processes [4]. Each primary electron can potentially liberate more than one secondary, and providing they are sufficiently energetic, these secondaries can excite other electrons by means of a cascade generation process. At each collision the electrons lose energy, and eventually they thermalise to the bottom of the conduction band. At this stage, the emission of electrons depends only on the ability of the low-energy electrons to overcome the energy barrier present at the surface. The total SEY ( $\delta$ ), is generally defined as the ratio of the number of emitted electrons or total emitted secondary electron current,  $I_s$ , to the number of incident electrons or primary electron current,  $I_p$ :

$$\delta = I_s/I_p. \quad (1.1)$$

Diamond presents, among other extraordinary properties, excellent electron emission characteristics, exhibiting higher yields than metals and many insulator materials [5–8] with values as high as 80 at 3 keV reported for pristine single-crystal diamond [9, 10] and  $\sim 10$  for polycrystalline films made by chemical vapour deposition (CVD) [11]. Previous studies demonstrate that high electron emission yields can usually be obtained from semiconducting boron-doped diamond films with hydrogen termination [12–14]. This is attributed to the combination of efficient electron transport from the region where the secondary electrons are generated to the surface, resulting in a large mean escape depth (around a few tens of nm for a primary energy,  $E_p \sim 1$  keV), together with a negative electron affinity (NEA) surface which removes the potential barrier for emission [5]. In addition, CVD diamond films have recently become widely available at relatively low cost, are robust, and compatible with Si fabrication technology which makes them easy to incorporate into existing dynode devices. Its potential for high yield offers several advantages for such devices including high time resolution, fast signal rise time, reduced pulse-height distribution, low noise, and chemical stability [11, 15].

In this paper we describe a custom-designed apparatus for the measurement of SEYs from thin chemical vapour deposition (CVD) diamond membranes. It uses a system of phosphor screens (PS) acting as detectors in association with PMTs to measure SEY. Design criteria and the procedures employed to calibrate the new system are presented along with preliminary test data.

## 2 Experimental

### 2.1 Faraday cup system

The most commonly used method for the determination of total SEYs involves measuring  $I_p$  and  $I_s$  using a conducting metal hemispherical Faraday Cup (FC) as a collector, as shown in figure 2. We used a FC system mounted inside a JEOL JSM-6100 scanning electron microscope (SEM) as a standard with which to compare the SEY measurements taken in our new phosphor-screen system (described in section 2.2).

In this FC system, a 0.5 mm-diameter aperture was positioned in the centre of the FC to allow the primary electron beam to pass through and strike the sample within. The measurements were performed under high vacuum ( $< 10^{-6}$  torr). The substrate was mounted on a biased stage which could be moved in the  $x$ ,  $y$  and  $z$  directions to enable the electron beam to strike different regions of the sample. The specimen was bombarded with high energy ( $\sim$  few keV) primary electrons produced by an electron gun which was focused through this hole and onto the sample surface. Accurate positioning of the electron beam was achieved by slowly rastering the beam and observing the image of the surface created by electrons reflected back up through the hole and onto the SEM detector. A sharp image of the surface meant that the beam was focused onto the sample surface with an estimated spot diameter of  $\sim 5$ –10 nm. To measure the SEY, the rastering of the beam was switched off allowing the focused, steady electron beam to strike the surface. The electron beam current could be controlled between  $4 \times 10^{-12}$  A to  $1 \times 10^{-11}$  A with primary energies,  $E_p$ , in the range of 0.6–10 keV. The resulting secondary electrons were emitted from the surface in a cosine distribution and were collected by the internal side of the Faraday cup, and measured as a total current. In this way, nearly all the emitted electrons were collected independently of the direction in which they were emitted.

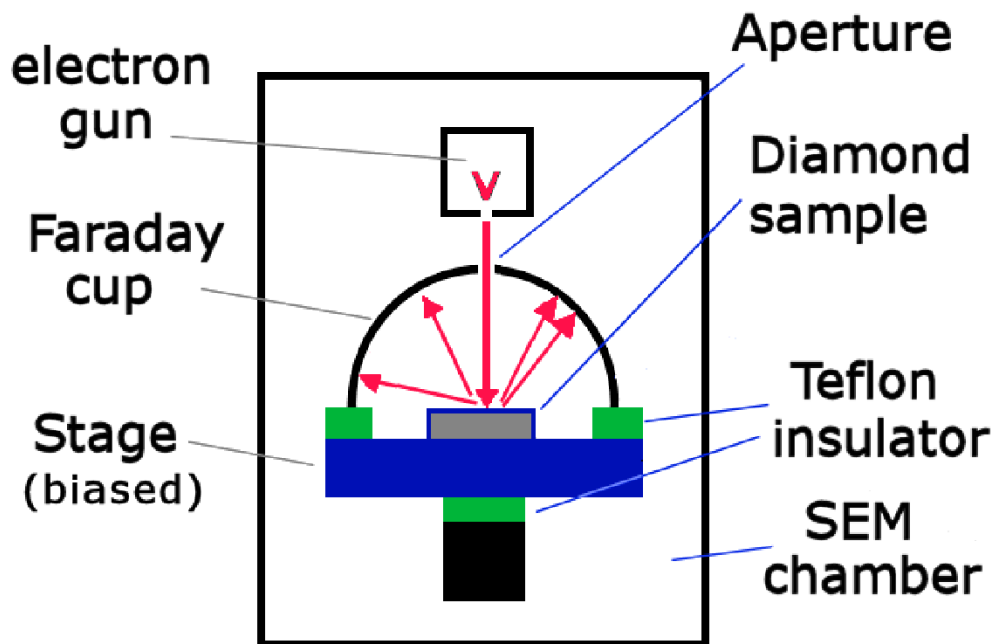


**Figure 2.** Schematic diagram of the conventional FC system used in Bristol as a standard with which to compare SEY yields. Design adapted from [16].

A bias voltage was applied to the substrate stage to overcome the possibility of surface charge effects which may impede other electrons from being emitted from the surface, causing a barrier for further emission. To do so, a sufficient bias was applied to overcome the work function difference between the sample and the FC. Voltages ranging in magnitude from 10 V to 30 V were evaluated. It was established that a bias of +20 V was sufficient to prevent charging, and this also forced the emitted low-energy secondary electrons to return to the sample surface, while the higher energy reflected primary electrons still reached the FC and were collected. Biasing at  $-20$  V repelled all secondary electrons away from the substrate and onto the FC. However, the current collected was then composed of two components; the true secondary electron current (with energies usually  $< 20$  eV) and the reflected primary electron current (with energies  $< E_p$ ). By measuring the currents recorded with each bias polarity in turn, the magnitude of the two components could be determined by subtraction.

In this system the SEY is measured as a function of primary electron energy,  $E_p$ , and is calculated from

$$\delta(E_p) = (I^- - I^+)/I \quad (2.1)$$

where  $I^-$  and  $I^+$  are current measured under the negative and positive biasing, respectively, and  $I$  is the incident current.

The advantages of the FC system is that it measures the total SEY directly without the need for complicated calibration, and it can be retrofitted into an existing SEM. The main limitation of this system, however, was that below  $E_p \sim 600$  eV secondary electron emission was greatly reduced, and the tiny current captured by the FC became almost equivalent to the noise in the system. Thus, current measurements below 600 eV were inaccurate and inconsistent, which is inconvenient

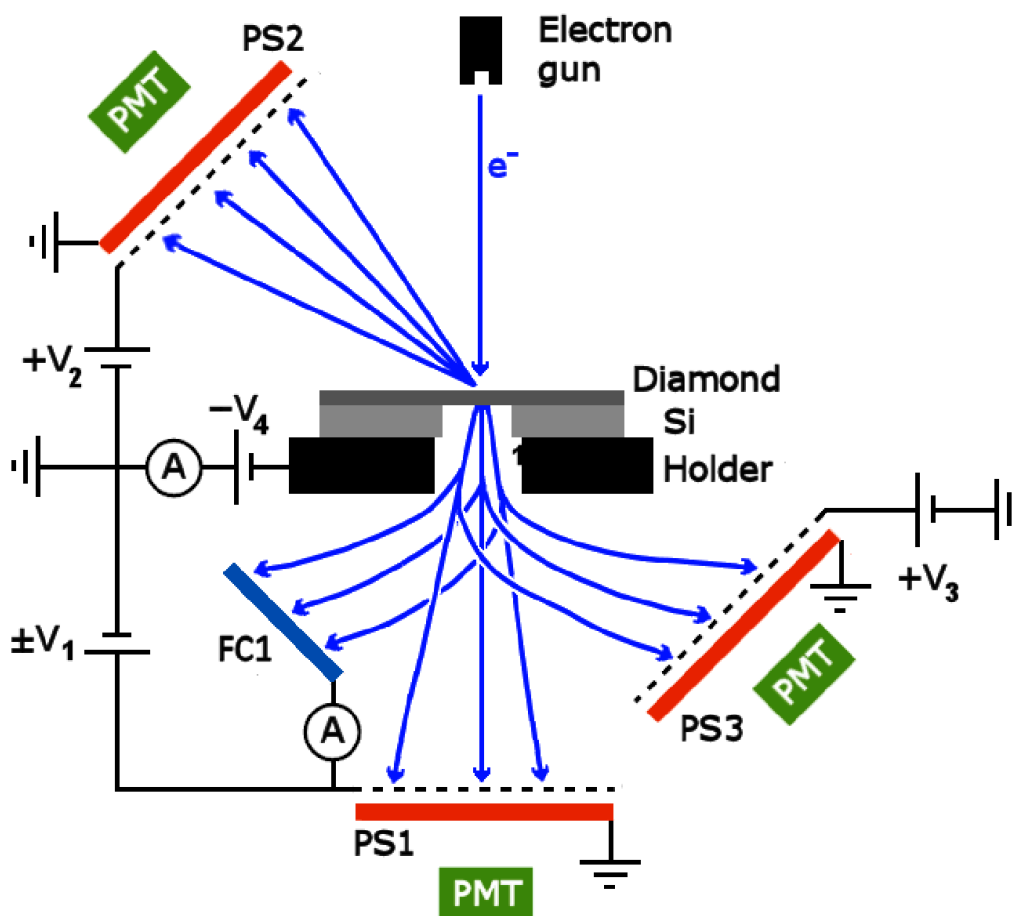


**Figure 3.** Schematic diagram of the setup adopted for reflection and transmission measurements using a system of PS and PMTs. The grids in front of each PS may be biased if required, as well as the Faraday Cup (FC1). Typical values for the bias voltages are:  $V_1$  +500 V (for FC or for enhanced collection of transmitted primary electrons on PS1), 0 to  $-500$  V (for use of PS1 as a retarding field analyser);  $V_2, V_3$  +500 V;  $V_4$   $-10$  V. The sample shown is a diamond membrane deposited onto Si, with an aperture etched into the back of the Si.

considering this is close to the peak of the SEY curve for diamond, meaning the important details of the low-energy SEY curve could not be obtained. This limitation can be removed, of course, by using a bespoke SEY testing rig with a low energy gun, as reported in ref. [11].

## 2.2 New Phosphor Screen system

A schematic diagram of the new SEY measurement system is shown in figure 3. It used a Kimball Physics EGL-2022 electron gun to generate primary electrons with acceleration energies controllable from 50 eV up to 5 keV, and beam currents from 1 nA to 500  $\mu$ A. The beam current from this was checked weekly using a FC and Keithley 2000 ammeter. The measured current was found to be within 1% of the value displayed on the Kimball output meter, which meant that this could be taken to be a representative value for  $I_p$ .

The electron gun was fitted to a custom-designed vacuum chamber operating at a base-pressure of  $\sim 10^{-6}$  torr. The electron source was oriented so that it would irradiate the surface of a diamond sample with primary electrons. The metal holder supporting the sample was connected to a d.c. voltage supply allowing it to be grounded or biased up to  $-20$  V, to repel any secondary electrons and also prevent them from being reabsorbed by the holder and substrate. When irradiated by primaries the secondary electrons emitted from the diamond sample surface were accelerated onto one of a number of Phosphor-coated Screen (PS) detectors, causing the screen to emit light. The PS were fabricated using a commercial cathodoluminescent phosphor coating, P22G (Nichia), emitting in the green with an emission peak at 530 nm. This phosphor powder is optimised for low-voltage operation by the incorporation of  $\sim 5\%$  submicron ITO particles. To fabricate the PS, a slurry of phosphor was applied to a glass plate to form a continuous submicron layer (corresponding to  $< 3$  phosphor-particle layers) and allowed to dry. This coating was deliberately thin to produce a saturated light output above a low threshold energy (see figure 4). A layer of gold ( $< 20$  nm) was evaporated onto the surface of the phosphor and connected to an electrical ground. The gold layer was too thin to affect electron transmission, but was needed to increase the phosphor surface conductivity to prevent the build-up of charge on the surface, and also allowed the PS to operate at voltages well below its typical operating range. Immediately in front of the gold-coated PS a fine gold mesh was mounted to which a bias voltage of up to  $+500$  V was applied, this ensured that all secondary electrons within a defined cone-angle were collected by the PS. Before each run checks were made to ensure that any leakage currents were negligible.

The light response from the PS was acquired as an electrical signal using a photomultiplier tube (PMT). The signal was fed into an analogue-to-digital card (National Instruments 6024E) and processed using a *Labview* computer program. The light emitted by each PS had an intensity that was proportional to the number of electrons that were incident on the phosphor, but was also a function of their kinetic energy. To determine this function, the electron gun was positioned to strike the phosphor screen directly, while the PMT signal versus  $E_p$  was measured for energy values from 20 eV to 5000 eV.

Figure 4 shows the results of the calibration experiment. For beam energies above 500 eV the PMT response curve (a) saturates at a maximum value, the magnitude of which depends linearly upon the chosen beam current as shown in inset (c). But for beam energies below 500 eV (b) the detection efficiency drops off approximately linearly with energy, down to  $\sim 20$  eV which was the lowest value for which the PS produced sufficient light intensity to be measurable on the PMT. Thus, biasing the PS grids at  $> +500$  V ensured that all slow-moving electrons would be accelerated towards the phosphor screen with energies approaching 500 eV, and thus that the PMT response was saturated and independent of the electron kinetic energy. This resulted in the PMT signal being only proportional to the number of electrons striking the phosphor, as required.

In the reflection configuration, the secondary electrons emitted from a sample surface normal to the primary electron beam were collected by a phosphor screen (PS2) positioned at  $\sim 45^\circ$  relative to the emission surface (see figure 3). By collecting at this angle nearly all the high energy reflected (backscattered) primary electrons were excluded, since they were mostly reflected in a cone with angle  $10^\circ$  to the normal incident beam. In contrast, the slower secondary electrons were emitted with a cosine distribution at energies  $< 20$  eV, and were then accelerated by the  $+500$  V potential on the grid to strike PS2.

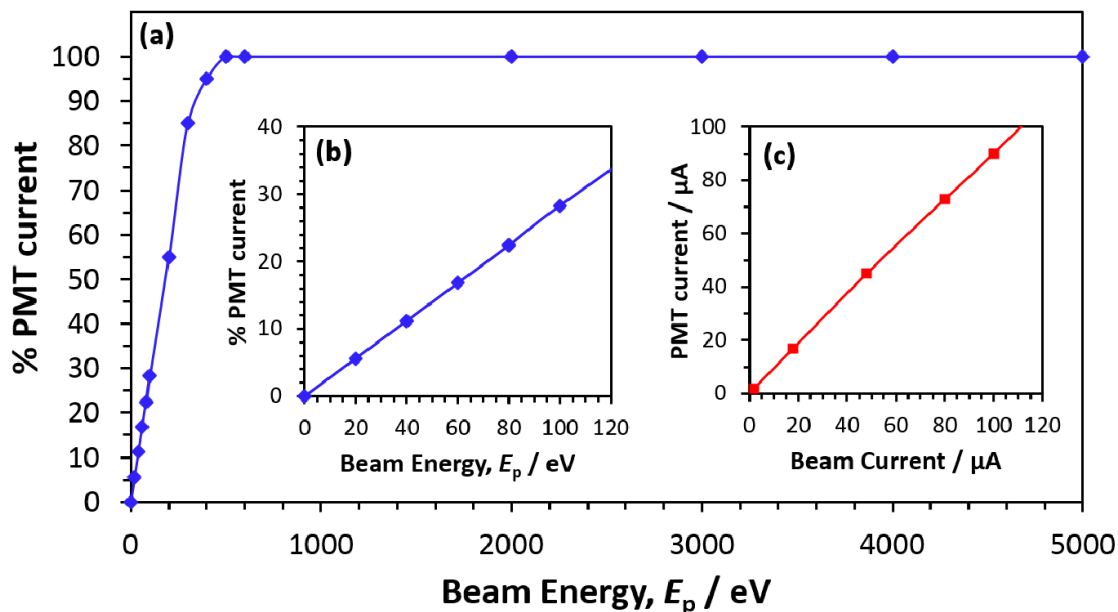


**Figure 4.** Calibration plots for the signal measured on the PMT as a function of electron beam energy,  $E_p$ , striking the PS. The main plot (a) shows that for  $E_p > 500$  eV the response of the PMT is constant and saturated at a maximum value, the magnitude of which depended upon the gain setting of the PMT. The inset (b) shows that for  $E_p < 500$  eV there is approximately a linear relationship between measured PMT current and  $E_p$ . The inset (c) shows that the maximum PMT signal depended linearly on the chosen beam current.

Before collecting SEY data, it was necessary to ensure that the electron beam was positioned correctly on the part of the sample surface under investigation. This was achieved by directly imaging the reflected electrons. In ‘imaging mode’, the electron beam was slowly rastered in the  $x$  and  $y$  directions across the surface of the sample holder, stopping at regular intervals to allow the intensity on the PS to be logged at that position. *Labview* software plotted these data as an image in real time, with the intensity forming the pixel brightness at the corresponding  $x, y$  position (see figure 5(a)). When the image was complete, it was possible to identify a region of interest on the sample, and then set the correct voltages on the e-beam deflection plates to ensure that the beam struck the desired location. This could be achieved with a lateral resolution of  $\sim 100 \mu\text{m}$ . Thus, imaging mode may be compared to a very slow, very low resolution *in situ* SEM, but was found to be essential when attempting to acquire SEY data from small features on a large mostly featureless sample. It should be noted that the voltage sampling rates for the PS/PMT are determined by the DAQ card (NI-6024E) which can support rates as high as 200,000 samples per second. For the imaging mode, a rate of 20,000 sample  $\text{s}^{-1}$  was chosen with an average signal value taken for each 100 voltage samples. This may be contrasted with the method of measuring signal current from the FC that used a Keithley 2000, and which can sample current values at only 2000 samples  $\text{s}^{-1}$ . To obtain a comparable signal voltage resolution as the PS/PMT the sampling rate would be only 5 samples  $\text{s}^{-1}$ . This means that it would be impractical for the FC detector to collect the large number of data points needed to acquire a scanned image with an equivalent resolution to the PS/PMT.

For transmission mode, thin membranes of diamond (typically  $\sim 2 \times 2$  mm) supported by a surrounding Si substrate ( $1 \text{ cm}^2$ ) were prepared (see section 2.3). The membrane sample was

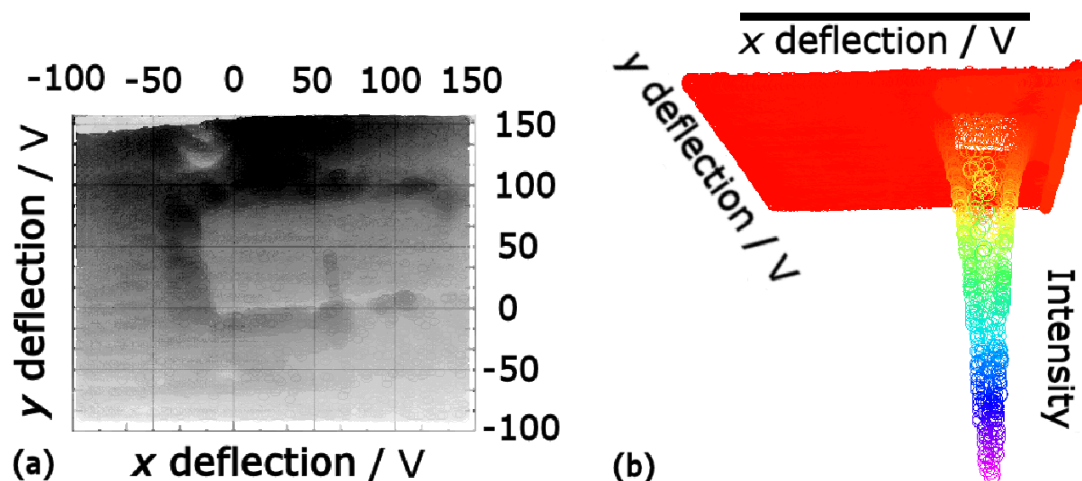


**Figure 5.** (a) A 2D image taken in ‘imaging mode’ of two square diamond samples sitting side-by-side on the substrate holder acquired in reflection mode. Sample size  $1\text{ cm}^2$ . The observed intensity at each point is related to the number of primary electrons scattered from the surface. (b) A 3D image of the intensity profile through a single square  $2 \times 2\text{ mm}$  diamond membrane obtained in transmission mode.

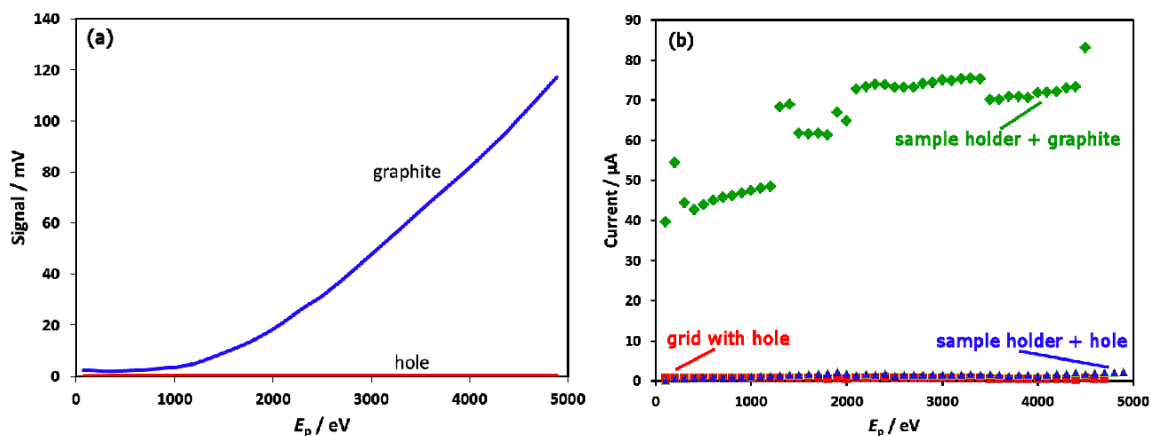


**Figure 6.** (a) Measurement of the signal from a substrate holder containing a graphite sample  $S_{\text{graphite}}$  and a similar-sized hole,  $S_{\text{hg}}$  measured in reflectance using PS2. (b) The current at the sample holder with the electron beam striking a graphite sample and a hole, and the current measured with a grid placed where PS2 usually sits, with the beam striking the hole. The beam current was  $80\text{ }\mu\text{A}$ .

then placed onto a substrate holder (details given below) which had a hole in the centre, with the membrane positioned over the hole. Two phosphor screens (PS1 and PS3) with 2 PMTs, plus a Faraday Cup (FC1) were positioned beneath this hole (see figure 3). Imaging mode was again used to ensure the electron beam was located correctly on the membrane, but an additional imaging mode using the signal from PS1, was now available. ‘Transmission imaging mode’ could generate simple two-dimensional images of the membrane, or alternatively, the intensity at each  $x, y$  position could be plotted in the  $z$  direction to make a three-dimensional representation of the transmittance through the membrane, as shown in figure 5(b). This could be used to check the thickness uniformity of the membrane or to locate the beam position for maximum signal. Because the transmission PS and

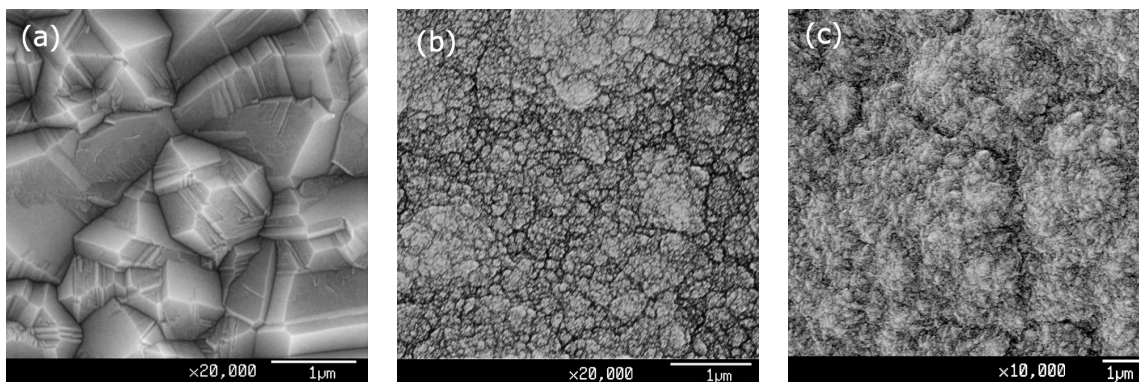


**Figure 7.** SEM micrographs of the morphology of (a) MCD, (b) NCD and (c) UNCD films grown on Si substrates.

reflection PS operated independently, the reflection yield could be obtained from the membrane samples at the same time as the transmission yield. This allows the relative number of electrons passing through each face of the membrane to be determined, which is crucial information for the design of in-line transmissive dynode devices.

One consideration for transmission mode is that PS1, which is in direct line-of-sight to the electron gun, collects both the high-energy primary transmitted electrons as well as the lower energy secondaries. To separate these two components, a third phosphor screen (PS3), grid and PMT were placed at  $45^\circ$  to PS1. Biasing the grid in front of PS3 at  $\sim +500$  V attracts the slower secondary electrons to PS3 while the faster primary electrons are barely deflected and continue onwards to strike PS1. In this way PS1 detects the primary electron signal while PS3 detects the secondary electron signal. The grid in front of PS1 is optional, but can be biased positively to help collection efficiency, or negatively so it can act as a retarding field analyser to obtain the energy distribution of the primaries. As an additional calibration source, a small Faraday Cup (FC1) was added, also placed at  $45^\circ$  to PS1, but on the opposite side of the sample to PS3. Biasing FC1 at  $+500$  V while PS3 was turned off allowed the absolute secondary electron current to be measured and this was used to calibrate the signal intensity seen on PS3.

The samples were mounted with conductive silver paint onto a copper-plate substrate holder. The holder was usually biased at  $-10$  V to repel any slow-moving secondary electrons away from the surface to prevent them being reabsorbed and lost as a contribution to the SEY signal. One potential problem with having a metallic substrate holder is that, no matter how well focused the electron beam, it is very difficult to prevent some fraction of the beam from striking the substrate holder and/or surroundings rather than just the sample. Thus, some unknown fraction of the measured secondary electron signal might not originate from the sample, and so needs to be subtracted to obtain the true SEY. This was achieved by coating the substrate holder and all components within the chamber that might be exposed to the electron beam with a thin layer of graphite. The graphite coating was prepared from graphite powder in aqueous solution which was applied to the surfaces and left to dry for a couple of hours. Graphite is often used as a plasma limiter at the walls of reactors to control the impurity flux [17] because it is one of the poorest secondary electron emitters having maximum SEY values of only 0.45–1.0 [18]. As such, graphite should suppress any sources of reflected electrons without compromising the electrical back contact of the samples.

### 2.2.1 Measurement procedure — reflection mode

The measurement procedure for obtaining the reflection SEY from a diamond sample involved loading 3 samples into the chamber: the diamond sample to be measured, and two calibration samples (one copper, one graphite) with SEY values known from prior measurements or literature reports. First, the electron gun was positioned onto the graphite sample and its signal response,  $S_g$ , for  $E_p = 0.2\text{--}5$  keV was measured, such that

$$S_g = S_{\text{graphite}} + S_{\text{bg}} \quad (2.2)$$

where  $S_{\text{graphite}}$  is the true signal from the graphite sample and  $S_{\text{bg}}$  is the unknown contribution to the total signal obtained from backscattered electrons that have been emitted from the substrate holder, mount and surroundings. Next, the beam was centred on the diamond sample to measure  $S_d$  (eq. (2.3))

$$S_d = S_{\text{diamond}} + S_{\text{bg}} \quad (2.3)$$

where  $S_{\text{diamond}}$  is the signal from the diamond sample and  $S_{\text{bg}}$  is the same background as before. Hence, the SEY is given by

$$\delta_{\text{diamond}} = \delta_{\text{graphite}} \times (S_d/S_g) \sim \delta_{\text{graphite}} \times (S_{\text{diamond}}/S_{\text{graphite}}). \quad (2.4)$$

The approximation in eq. (2.4) is valid only if the background signal is much smaller than the signal emitted by the diamond sample (i.e. if  $S_{\text{bg}} \ll S_{\text{diamond}}$ ). This is reasonable given the relative magnitudes of the SEY values for diamond ( $> 10$ ) and the graphite-coated surroundings ( $< 1$ ). If we estimate that 5% of the focused electron beam would strike the surroundings (which seems rather pessimistic for such a well-confined beam) then  $S_{\text{bg}} : S_{\text{diamond}} = 1 : 200$ . However, the energy dependence of  $\delta_{\text{diamond}}$  is not necessarily identical to that of  $\delta_{\text{graphite}}$ , so we must alter the by replacing  $\delta_{\text{graphite}}$  with  $\delta_{\text{graphite}}(E_p)$  which corresponds to the yield measured for the graphite sample for each primary energy,  $E_p$ . So, a more accurate expression for the SEY is given by:

$$\delta_{\text{diamond}}(E_p) \sim \delta_{\text{graphite}}(E_p) \times (S_d/S_g). \quad (2.5)$$

Neither the maximum yield value nor the primary energy at which it occurs is affected by this correction; the only effect is that the yield curves after correction are slightly narrowed. The correction factor  $\delta_{\text{graphite}}(E_p)$  at each value of  $E_p$  was taken from fitting the known experimental and theoretical yield curves for graphite [11, 17–21]. Again, these considerations are reasonable due to the very small yield of graphite, equalling unity at most [11].

In addition, in order to validate the assumption that  $S_{\text{bg}} \ll S_{\text{diamond}}$  the background signal was measured directly using a metal plate containing a  $1 \text{ cm}^2$  aperture, representing the area that would normally be occupied by a sample. With the electron beam centred on this aperture, the only secondary electrons that could be detected were those created by that small portion of the beam that did not go down the hole, but instead struck the surroundings. Thus, this was a direct measure of  $S_{\text{bg}}$  which is plotted in figure 6(a) alongside the signal from a graphite substrate. It is clear that the background signal is very small compared to the signal from graphite, which itself is  $\sim 10$  times smaller than the signal from diamond (depending on beam energy).

As a further check, the experiments were repeated except this time measuring directly the current generated in the substrate holder with the graphite sample present and with just the aperture,

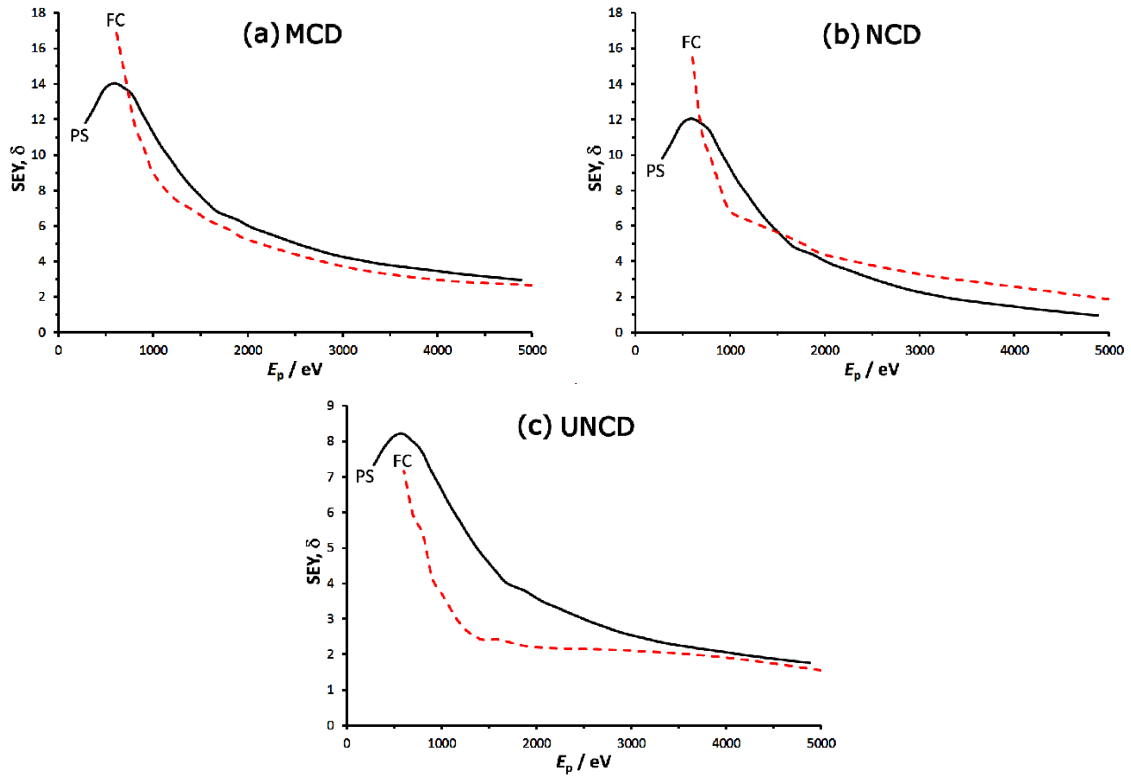


**Figure 8.** Comparison of reflection SEY measurements made at Bristol using the PS setup with those obtained with the in-house FC (as in figure 2) for (a) MCD, (b) NCD and (c) UNCD, films on Si substrates.

as shown in figure 6(b). With the hole present, the majority of the primary electron beam passes straight through without striking the substrate holder, and so the current measurement gives an indication as to what fraction of the beam actually struck the substrate holder. It is clear from the relative size of the two currents that a negligible amount of the beam current strikes the substrate holder. A third experiment was performed by replacing PS2 with a positively biased metal-grid collector to record the relative current from any secondary electrons generated from the surroundings when the beam passed through the hole. Again, from figure 6(b) this current is negligibly small.

These combined results suggest that the approximations that  $S_{bg} \ll S_{diamond}$  and that  $S_{bg} \ll S_{graphite}$  are valid, and that in the energy range we have used,  $S_{bg}$  is negligible. Thus, the value for  $\delta$  for the diamond sample calculated from eq. (2.5) should be reliable.

In order to convert the relative signal from the PS into a quantitative SEY, the beam was then positioned to strike the calibration sample (graphite or copper), and the SEY signal as function of  $E_p$  was measured. A similar correction was applied, namely:

$$S_{Cu} = S_{copper} + S_{bg} \quad (2.6)$$

$$\delta_{copper}(E_p) \sim \delta_{graphite}(E_p) \times (S_{Cu}/S_g) \quad (2.7)$$

Copper was chosen as the calibration sample because it exhibited a much higher yield (between 1.5 and 2) than graphite and so more closely resembled diamond. The curve obtained for  $\delta_{copper}(E_p)$  was then compared against the reference value [22], and, where necessary, the curve was multiplied

by a constant correction factor,  $k$ , to scale the measured curve to fit the reference. This adjustment was needed to remove any day-to-day variations in signal levels from the PS or PMTs. Typically  $k$  was between 0.95 and 1.05, suggesting a 5% variation. There are a number of SEY measurements for Cu in the literature which could have been used as a reference. There is also a substantial variation in the published SEY data because emission is so sensitive to the surface quality; contamination by minute levels of impurities, oxidation, or even primary electron irradiation. We have chosen to use the SEY curve in ref. [22] as our reference as the measurements were taken over the same energy range as our system, and under broadly similar conditions.

Once the primary electron beam was correctly positioned and focused onto the diamond sample, reflection mode measurements were recorded. The SEY values were calculated using eq. (2.5) and then multiplied by  $k$  to give the final calibrated SEY for each primary energy value.

### 2.2.2 Measurement procedure – transmission mode

The measurement procedure for obtaining the transmission SEY from a thin diamond sample involved placing the sample, usually a diamond membrane supported by a surrounding Si frame (see section 2.3), onto the holder, and positioned directly above a hole. Imaging mode was used to locate the position of the membrane and the  $x, y$  coordinates of the centre of the membrane noted. To obtain a value for the primary beam current signal,  $S_p$ , the beam was steered to avoid the sample completely and strike PS1 directly. Steering the beam back to the centre of the membrane allowed the total transmitted current,  $S_{\text{tot}}$ , to be measured, which consists mainly of the transmitted high-energy primaries (if any) plus slower secondaries. Because the position of the beam moved slightly as the primary energy was changed, the beam was re-centred manually at every beam energy by steering its  $x, y$  position slightly until maximum transmitted signal was achieved on PS1.

To separate  $S_{\text{tot}}$  into its two components, the grid in front of PS1 was grounded while that in front of PS3 was biased at +500 V. In this way, any high-energy primaries were detected on PS1, while simultaneously the slower secondaries were attracted and accelerated onto PS3. To obtain an absolute magnitude for the signal on PS3, its grid was grounded and instead the Faraday Cup (FC1), placed in the identical location but facing PS1, was biased at +500 V and the signal collected. Once this had been performed for a range of different signal levels, the response of PS3 was calibrated and could be used from then onwards for all subsequent samples without further need of FC1.

## 2.3 CVD Diamond test samples

For reflection mode, three different types of CVD diamond film were deposited using a hot filament CVD reactor and standard deposition conditions [23] of 20 torr pressure, Ta filament at 2400 K positioned 3 mm above the pre-abraded Si substrate, 7 h deposition time, which produced undoped polycrystalline diamond films  $\sim 3 \mu\text{m}$  thick. The gas mixture ( $\text{CH}_4/\text{H}_2/\text{Ar}$ ) was varied to produce films with different grain sizes. A gas mixture of 1:100:0, respectively, produced microcrystalline diamond (MCD) films with faceted crystals of size  $\sim 2 \mu\text{m}$ . Increasing the methane percentage (4:96:0) reduced the grain size to  $\sim 100 \text{ nm}$  and produced nanocrystalline diamond films (NCD), with the grains becoming rounded or ‘cauliflower’ in morphology. For a gas composition of 1:1:98, so-called ultra-nanocrystalline diamond (UNCD) films were produced, with grain size  $< 10 \text{ nm}$  and with a very smooth, flat surface. Due to the slower growth rate for UNCD, these films were only

0.5  $\mu\text{m}$  thick. The number of grain boundaries, and hence the proportion of  $sp^2$  graphitic impurities, increased significantly on going from MCD to NCD to UNCD, whilst the film roughness increased in the opposite direction. These films were all undoped, and so were electrically insulating, although they all had hydrogen-terminated surfaces creating slight conductivity across the surface due to surface transfer doping [24]. Examples of the morphologies of these three film types are shown in figure 7.

In order to compare how the values measured using our new PS system compared with those measured using a more conventional FC system, two boron-doped diamond samples were made for comparison with a bespoke FC system based at Leicester University, and described in detail elsewhere [11]. The diamond was doped with B to prevent the samples charging up. These films were  $\sim 2.5 \mu\text{m}$ -thick NCD grown on Si, using  $\text{B}_2\text{H}_6$  gas as the boron source, and had the same morphology as the undoped NCD film shown in figure 5(b). The two films differed only in their B content and 2-point electrical resistance, which were 5 k $\Omega$  and 170 k $\Omega$ , respectively.

For transmission mode, thin membranes of diamond (typically  $\sim 2 \times 2 \text{ mm}$ ) supported by a surrounding Si substrate (1  $\text{cm}^2$ ) were required. These were purchased from Applied Diamond, Inc., with a range of membrane thicknesses from 20 nm-200 nm. Other samples were made in house, by depositing thin CVD diamond samples onto a Si surface and then selectively etching away a window in the backside of the Si to expose the membrane. The details of this procedure are given elsewhere [25].

### 3 Results

#### 3.1 SEY measured in Reflection Mode

Figure 8 shows the reflection SEY values measured as a function of  $E_p$  for the three diamond samples shown in figure 7. For energies  $E_p > 1 \text{ keV}$  the SEY values measured using the in-house FC (as in figure 2) are very close to the values measured using the new PS system. The obvious difference between the two systems comes at lower energies, where the FC system cannot measure values at  $E_p < 600 \text{ eV}$  due to the limitations of the electron gun in the SEM. This is problematic because the maximum in the yield curve occurs at  $\sim 500\text{--}1000 \text{ eV}$  for the three diamond film types, and therefore this peak cannot be discerned using the conventional FC system. The PS system, however, displays this peak nicely, although the maximum SEY is quite a bit lower than that measured with the FC. This could be because at these low primary energies a greater number of secondary electrons have very low or near-zero energy. These electrons would eventually still be counted by the FC, but depending upon the grid voltage, would stand an increased chance of drifting away from the PS detectors, striking the surroundings to be lost to ground. Thus, at low energies the PS system appears to underestimate the maximum yield by  $\sim 15\text{--}20\%$ . With this knowledge, subsequent yield curves can be corrected by this amount to obtain data consistent with FC measurements.

Figure 8(c) shows that the response from UNCD has a slightly different behaviour than the other two films, with the signal from the FC being reduced compared to that from the PS. The reason for this is unclear, however the UNCD films were considerably thinner than the other two films, and there is a possibility that more of the primary electrons transmitted through the diamond film

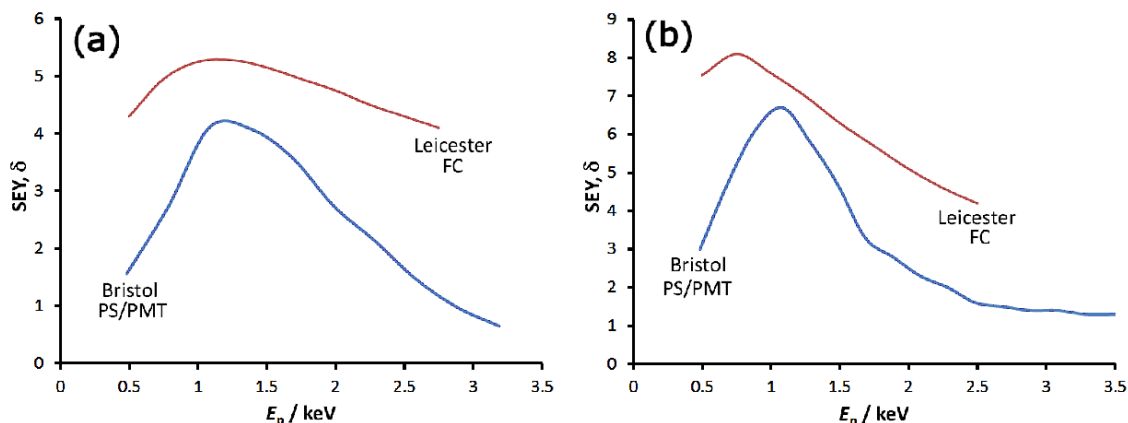


**Figure 9.** Reflection SEYs measured from two different CVD diamond samples in the Bristol University PS/PMT and Leicester University FC systems. The samples were  $2.3 \mu\text{m}$  B-doped diamond films grown on p-type Si, with differing B concentrations. (a) Heavily B-doped diamond with a 2-point resistance of  $5 \text{ k}\Omega$ , whilst (b) was lightly B-doped diamond with a resistance of  $170 \text{ k}\Omega$ .

into the underlying Si substrate. Si has a lower SEY than diamond, so fewer secondary electrons will be generated from primaries that reach the Si layer, reducing the apparent SEY. Although this might explain why the overall signal is smaller for UNCD, it does not really explain why the two systems measure different values. This is currently under investigation.

Figure 9 shows the experimental results obtained with the two B-doped CVD diamond films tested both in the Bristol University PS/PMT and Leicester University FC equipment. The results indicate that the new PS/PMT system produces a similar SEY profile, but the SEY values obtained for a given primary energy are on average 10–20% lower than those recorded in the Leicester FC system. The reason for this difference is not clear, but since it is similar in magnitude to the offset observed when comparing FC and PS measurements made in the same apparatus, the same correction offset can be applied to account for this.

The curves from figures 8 and 9 reveal that the two boron-doped diamond SEY curves peak at higher energies ( $\sim 1.2 \text{ keV}$ ) compared to those for the three undoped diamond samples ( $\sim 700 \text{ eV}$ ), although the peak SEY values are lower (4–6 compared to 8–14). These features are probably related to the higher conductivity of the B-doped films allowing more electrons to escape from deeper in the film, and will form the basis of a future systematic study of the effect of conductivity on SEY.

### 3.2 SEY measured in Transmission Mode

Figure 10 shows an example of transmission SEY as a function of beam energy for a 400-nm-thick undoped MCD diamond membrane. An analysis using the Kanaya and Okayama equation [26] for electron range,  $R$ , in solids:

$$R(/\mu\text{m}) = (0.0276AE_p^{1.67})/(Z^{0.889}\rho) \quad (3.1)$$

where for diamond  $A = 12$ ,  $Z = 6$ , and  $\rho = 3.51 \text{ g cm}^{-3}$ ,  $E_p$  is in keV, and 0.0276 is a scaling factor to give the range in  $\mu\text{m}$ , shows that for the maximum primary energy used ( $5 \text{ keV}$ ) the electrons

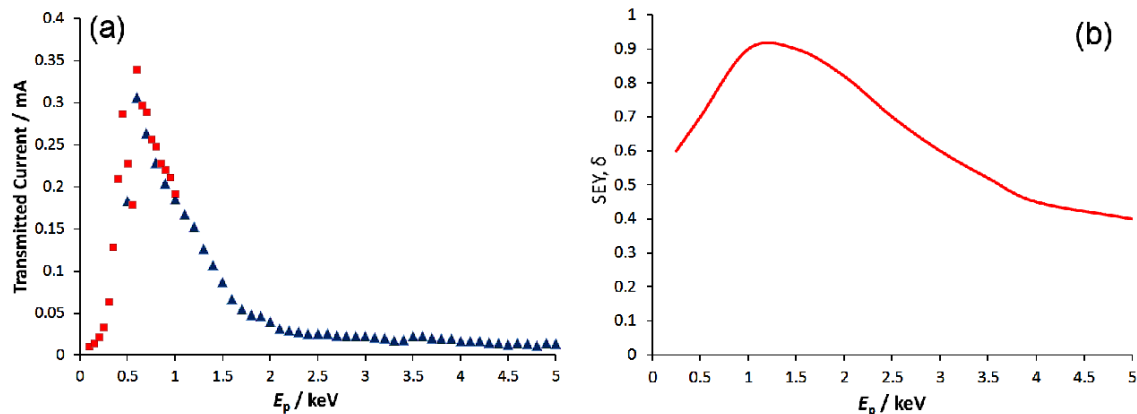


**Figure 10.** Transmission electron yields from a 400-nm-thick undoped diamond membrane. (a) The raw transmitted current with increasing primary energy,  $E_p$ , measured using FC1 (red squares) and decreasing primary energy measured using PS3 (blue triangles). The curve from PS3 has been normalised to the same maximum current as that from FC1 to allow comparison. (b) The transmission SEY curve after data processing and calibration.

will penetrate  $\sim 280$  nm. Although this is less than the thickness of the membrane, uncertainties in the accuracy of the membrane thickness ( $\pm 100$  nm from SEM measurements) and approximations inherent in eq. (3.1) mean that some transmitted primary electrons might also contribute to, and potentially overwhelm, the small measured SEY signal on PS1. Therefore, SEY measurements were made using the offset biased screen PS3 or FC1.

Figure 10(a) illustrates how the raw transmission currents measured using PS3 with decreasing beam energy compare with those measured using FC1 with increasing beam energy. The curve from PS3 has been normalised to the same maximum current as that from FC1, so that a comparison between the two curves can be made. Clearly, once this normalisation of the absolute signal has been done, the curves measured by both methods overlap well. Following background subtraction and calibration (as detailed in section 2.2), figure 8(b) shows that the absolute magnitude of the maximum SEY is  $< 1$ , probably due to the thickness of the diamond membrane. These values are consistent with those obtained by Yater et al. [27] who studied transmission yields from a 150-nm-thick B-doped diamond membrane and also obtained yields  $< 1$ . One of the practical difficulties encountered while measuring thin membranes was their susceptibility to perforation and disintegration during testing. The fragility of the membranes had a major impact upon the number of datasets acquired in transmission mode. The poor mechanical stability can be attributed to the method employed to selectively remove the silicon substrate supporting the diamond layer. Future studies will need to identify a way to resolve this issue.

## 4 Conclusions

A methodology has been developed for the acquisition and imaging of SEY data from thin diamond membranes. The setup consists of a system of phosphor screens acting as detectors, each of which is linked to a dedicated PMT for the acquisition of signals which are transferred to a computer via a *Labview* interface. One advantageous feature of this new system is that the beam can be navigated

across a sample surface and the reflected or transmitted electrons collected on a PS and viewed as an image on a computer screen in real time. This allows small features on a sample surface, such as locally thinned regions or voids, to be easily visualised and their  $x,y$  coordinates located, such that the beam can be steered to strike or avoid the feature of interest. This is particularly useful for non-homogeneous samples, or for locating the central position of small membrane structures for transmission mode measurements.

Preliminary SEY data have been presented for diamond samples recorded in reflection and transmission modes. The reflection SEY measured for two diamond samples in the new apparatus were compared with measurements of similar samples that were made in another laboratory using a conventional FC detector setup. On average, a difference of approximately 10–20% was found between those measured by our setup and by the FC method. Although the system has been developed for measurement of diamond samples with SEY values much larger than unity, it can be used for any material that has a reasonably high SEY.

In future experiments, we aim to report a comprehensive investigation of the reflection and transmission SEY values using diamond films with varying impurity dopant levels, morphology, thickness, surface termination, grain size and substrate material.

## Acknowledgments

The authors would like to thank AWE and STFC for funding this project.

## References

- [1] N. Getoff, M. Gerschpacher, J. Hartmann, J.C. Huber, H. Schittl and R.M. Quint, *The 4-hydroxyestrone: Electron emission, formation of secondary metabolites and mechanisms of carcinogenesis*, *J. Photochem. Photobiol.* **B 98** (2010) 20.
- [2] P. Bergonzo, D. Tromson, C. Mer, B. Guizard, F. Foulon and A. Brambilla, *Particle and radiation detectors based on diamond*, *Phys. Stat. Sol.* **A 185** (2001) 167.
- [3] H. Seiler, *Secondary electron emission in the scanning electron microscope*, *J. Appl. Phys.* **54** (1983) R1.
- [4] W.S.M. Werner, *Photon and Electron Induced Electron Emission from Solid Surfaces*, *Springer Tr. Mod. Phys.* **225** (2007) 39.
- [5] O. Auciello et al., *Are diamonds a MEMS' best friend?*, *IEEE Microw. Mag.* **8** (2007) 61.
- [6] W.S. Kim et al., *Secondary electron emission from magnesium oxide on multiwalled carbon nanotubes*, *Appl. Phys. Lett.* **81** (2002) 1098.
- [7] P. Ascarelli et al., *Secondary electron emission from diamond: Physical modeling and application to scanning electron microscopy*, *J. Appl. Phys.* **89** (2001) 689.
- [8] J. Cazaux, *Some considerations on the secondary electron emission,  $\delta$ , from  $e^-$  irradiated insulators*, *J. Appl. Phys.* **85** (1999) 1137.
- [9] A. Shih, J. Yater, P. Pehrsson, J. Butler, C. Hor and R. Abrams, *Secondary electron emission from diamond surfaces*, *J. Appl. Phys.* **82** (1997) 1860.
- [10] J.E. Yater, A. Shih and R. Abrams, *Electron transport and emission properties of diamond*, *J. Vac. Sci. Technol.* **A 16** (1998) 913.

- [11] J.S. Lapington et al., *Erratum: investigation of the secondary electron emission characteristics of alternative dynode materials for imaging photomultipliers*, [2012 JINST 7 E04002](#).
- [12] F.J. Himpsel, J.A. Knapp, J.A. VanVechten and D.E. Eastman, *Quantum photoyield of diamond(111) — A stable negative-affinity emitter*, [Phys. Rev. B 20 \(1979\) 624](#).
- [13] G. Piantanida et al., *Effect of moderate heating on the negative electron affinity and photoyield of air-exposed hydrogen-terminated chemical vapor deposited diamond*, [J. Appl. Phys. 89 \(2001\) 8259](#).
- [14] S. Michaelson, V. Richter, R. Kalish, A. Hoffman, E. Cheifetz and R. Akhvlediani, *Ion-induced electron emission from undoped sub-micron thick diamond films*, [Thin Solid Films 420–421 \(2002\) 185](#).
- [15] J.S. Lapington, P.W. May, N.A. Fox, J. Howorth and J.A. Milnes, *Investigation of the secondary emission characteristics of CVD diamond films for electronamplification*, [Nucl. Instrum. Meth. A 610 \(2009\) 253](#).
- [16] D.M. Trucchi, E. Cappelli, N. Lisi and P. Ascarelli, *Feasibility of CVD diamond radiation energy conversion devices*, [Diamond & Relat. Mater. 15 \(2006\) 1980](#).
- [17] H. Farhang, E. Napchan and B.H. Blott, *Electron Backscattering and Secondary Electron Emission from Carbon Targets: Comparison of Experimental Results with Monte-Carlo Simulations*, [J. Phys. D 26 \(1993\) 2266](#).
- [18] H. Bruining, *Physics and Applications of Secondary Electron Emission*, Pergamon Press, McGraw-Hill, New York U.S.A. (1954).
- [19] J. Cazaux, *Charging in scanning electron microscopy “from inside and outside”*, [Scanning 26 \(2004\) 181](#).
- [20] M.E. Woods et al., *An investigation of the secondary-electron emission of carbon samples exposed to a hydrogen plasma*, [J. Phys. D 20 \(1987\) 1136](#).
- [21] J.H. Jonker, *On the theory of secondary electron emission*, [Philips Res. Rep. 7 \(1952\) 1](#).
- [22] H. Bruining and J.H. De Boer, *Secondary electron emission: Part I. Secondary electron emission of metals*, Natuurkundig Laboratorium der N.V. Philips’ Gloeilampenfabrieken, Netherlands Physica, Eindhoven-Holland (1938).
- [23] P.W. May, *Diamond thin films: a 21st-century material*, [Phil. Trans. R. Soc. Lond. A 358 \(2000\) 473](#).
- [24] P. Strobel, M. Riedel, J. Ristein and L. Ley, *Surface transfer doping of diamond*, [Nature 430 \(2004\) 439](#).
- [25] R. Vaz, *Studies of the secondary electron emission from diamond films*, Ph.D. Thesis, School of Chemistry, University of Bristol, Bristol U.K.
- [26] J.I. Goldstein, D.E. Newbury, P. Echlin, D.C. Joy, C. Fiori and E. Lifshin, *Scanning Electron Microscopy and X-Ray Microanalysis*, Plenum Press, New York U.S.A. (1981), pg. 72.
- [27] J. E. Yater, A. Shih, J.E. Butler and P.E. Pehrsson, *Transmission of low-energy electrons in boron-doped nanocrystalline diamond films*, [J. Appl. Phys. 93 \(2003\) 3082](#).